A&A 585, A112 (2016)
DOI: 10.1051/0004-6361/201526271

Astronomy & Astrophysics

The sulfur depletion problem: upper limits on the H_2S_2, $HS_2^{\cdot}$, and S_2 gas-phase abundances toward the low-mass warm core IRAS 16293-2422⋆

R. Martín-Doménech[1], I. Jiménez-Serra[2,3], G. M. Muñoz Caro[1], H. S. P. Müller[4], A. Occhiogrosso[2], L. Testi[3], P. M. Woods[5], and S. Viti[2]

[1] Centro de Astrobiología (INTA-CSIC), Ctra. de Ajalvir, km 4, Torrejón de Ardoz, 28850 Madrid, Spain
e-mail: rmartin@cab.inta-csic.es
[2] University College London, 132 Hampstead Road, London NW1 2PS, UK
[3] European Southern Observatory, Karl-Schwarzschild-Str. 2, 85748 Garching, Germany
[4] I. Physikalisches Institut, Universität zu Köln, Zülpicher. Str. 77, 50937 Köln, Germany
[5] Astrophysics Research Centre, Dept. of Mathematics & Physics, Queen's University Belfast, Belfast BT7 1NN, UK

Received 7 April 2015 / Accepted 22 November 2015

ABSTRACT

Context. A fraction of the missing sulfur in dense clouds and circumstellar regions could be in the form of three species not yet detected in the interstellar medium: H_2S_2, $HS_2^{\cdot}$, and S_2 according to experimental simulations performed under astrophysically relevant conditions. These S-S bonded molecules can be formed by the energetic processing of H_2S-bearing ice mantles on dust grains, and subsequently desorb to the gas phase.

Aims. The detection of these species could partially solve the sulfur depletion problem, and would help to improve our knowledge of the poorly known chemistry of sulfur in the interstellar medium. To this purpose we calculated the frequencies and expected intensities of the rotational transitions not previously reported, and performed dedicated ground-based observations toward the low-mass warm core IRAS 16293-2422, a region with one of the highest measured gas-phase H_2S abundances.

Methods. Observations in the submillimeter regime were obtained with the APEX 12 m telescope during 15 h of observation. A total of ∼16 GHz were covered in a range of about 100 GHz, targeting a wide selection of the predicted rotational transitions of the three molecules.

Results. The 1σ noise rms values were extracted in the spectral regions where the targeted species should have been detected. These values were a factor of 2−7 lower than those reached by previous observations toward the same source, and allowed us to estimate a 1σ upper limit to their molecular abundances of $\leq 8.1 \times 10^{-9}$, $\leq 1.1 \times 10^{-8}$, and $\leq 2.9 \times 10^{-7}$ relative to H_2, for H_2S_2, $HS_2^{\cdot}$, and S_2, respectively.

Conclusions. The upper limit abundances of the three molecules containing the S_2 unit are up to two orders of magnitude lower than the H_2S abundance in the source, and one order of magnitude lower than the expected abundances from the experimental simulations using ice analogs. Subsequent gas-phase chemistry after desorption could lower the abundances of the three species to undetectable levels in our observations.

Key words. ISM: abundances – ISM: molecules – ISM: individual objects: hot corino – methods: observational – radio lines: ISM

1. Introduction

Sulfur, the tenth most abundant element in the Galaxy, is of particular interest from an astrochemical point of view. On the one hand it has been suggested that sulfur-bearing species can act as chemical clocks in star forming regions (Charnley 1997; Hatchell et al. 1998; Viti et al. 2001; Wakelam et al. 2004a, 2011). On the other hand, along with carbon, hydrogen, nitrogen, oxygen and phosphorus, it is one of the elements commonly present in molecules of biotic interest.

Previous observations have shown that sulfur is depleted in dense clouds and circumstellar regions around young stellar objects (YSOs). The S-bearing species already detected in these regions account for only ∼0.1% of its estimated cosmic abundance (1.23×10^{-5} N_H; Tieftrunk et al. 1994). It has been proposed that the missing sulfur is locked onto the icy mantles of dust grains (e.g., Millar & Herbst 1990; Jansen et al. 1995; Ruffle et al. 1999). Until now, only OCS (Geballe et al. 1985; Palumbo et al. 1995) and SO_2 (Boogert et al. 1997) have been firmly detected in icy grain mantles toward high-mass protostars, but their estimated abundances are on the order of ∼0.5%, and ∼0.8−4.0%, respectively, of the total cosmic S abundance (Boogert et al. 1997).

In cometary ices H_2S is the most abundant S-bearing molecule, with an abundance of up to 1.5% relative to water (Bockelée-Morvan et al. 2000), or 1.5×10^{-6} relative to H_2. The presence of H_2S in interstellar ices was inferred from IR observations toward the high-mass protostar W33A (Geballe et al. 1985). However, a robust detection of this molecule in interstellar ices has not been reported yet, probably because of the overlapping of the 3.92 μm IR band of H_2S with a strong IR feature of methanol. The upper limit found for this species toward dense

⋆ The reduced spectra for the observed 16 GHz at the original spectral resolution are only available at the CDS via anonymous ftp to cdsarc.u-strasbg.fr (130.79.128.5) or via http://cdsarc.u-strasbg.fr/viz-bin/qcat?J/A+A/585/A112

clouds and circumstellar regions ($0.6–1.6 \times 10^{-6}$, and $0.04–0.12 \times 10^{-6}$ relative to H_2, respectively; Smith 1991) accounts for only 10% of the cosmic S abundance.

A fraction of the H_2S present in interstellar ices could be energetically processed by UV-photons, X-rays, or cosmic rays in dense cloud interiors and regions around YSOs, leading to the formation of other S-bearing species. These new molecules would subsequently be released to the gas phase by means of photon or ion-induced desorption, and also thermal desorption in the hot regions of the circumstellar envelopes around YSOs, harboring part of the missing sulfur. This is indeed a very plausible scenario, since several of the gas-phase S-containing molecules already observed in hot cores, such as H_2S, SO_2, OCS, SO, H_2CS, HCS^+, and NS (van der Tak et al. 2003; Jiménez-Serra et al. 2012), have abundances that cannot be explained with gas-phase-only chemical models (Doty et al. 2004; Viti et al. 2004; Wakelam et al. 2004a). This scenario has been tested in the laboratory for the past thirty years. Experimental simulations of the irradiation of interstellar ices containing H_2S under astrophysically relevant conditions have been performed using UV photons (Grim & Greenberg 1987; Jiménez-Escobar & Muñoz Caro 2011; Jiménez-Escobar et al. 2014), X-rays (Jiménez-Escobar et al. 2012), or ions (Moore et al. 2007; Ferrante et al. 2008; Garozzo et al. 2010). Energetic processing of H_2S-bearing ices readily generates sulfur-sulfur bonds, and the main S-bearing products in these experiments are usually H_2S_2 and $HS_2^{\cdot}$. The molecule H_2S_2 can subsequently photodissociate forming S_2 and S_3, which have recently been detected by Jiménez-Escobar & Muñoz Caro (2011). These molecules with two S atoms could thus contain a significant fraction of the missing sulfur in dense clouds and circumstellar regions, but their observation in the solid or gas phase have not yet been reported.

Dense circumstellar envelopes around YSOs such as high-mass hot cores and low-mass warm cores (or hot corinos) are prime candidates for the detection of these S-bearing molecules in the gas phase, since ice mantles are largely affected by intense UV and/or X-ray irradiation from their central protostars before their thermal desorption. The low-mass warm core IRAS 16293-2422 (or hot corino) is known to show an active chemistry as demonstrated by its rich molecular line spectrum (Caux et al. 2011; Jørgensen et al. 2011). The derived gas-phase H_2S abundance toward this object is one of the highest measured in low-mass warm cores (5×10^{-7}; Wakelam et al. 2004b) and is therefore a good candidate to test whether an important fraction of the missing sulfur is contained in the form of any of these S-bearing species coming from H_2S. IRAS 16293-2422 is a binary system whose sources A and B are spatially separated by 5″ (Mundy et al. 1992). Among the two sources, IRAS 16293-2422 A shows a very rich sulfur chemistry with several sulfur-bearing molecules detected, such as H_2S, SO, SO_2, HCS^+, H_2CS, CS, and OCS (Wakelam et al. 2004b; Caux et al. 2011; Jørgensen et al. 2011). The measured rotational temperature of the hot corino is $T_{\rm rot} = 100$ K (Ceccarelli et al. 2000).

We present the first single-dish observations targeting a wide selection of the predicted rotational transitions for three of the products detected in the experimental simulations (H_2S_2, $HS_2^{\cdot}$, and S_2) toward IRAS 16293-2422. Although none of the three species was firmly detected, our observations provide stringent upper limits to their molecular abundances, constraining the efficiency of UV-photoformation of H_2S_2, $HS_2^{\cdot}$, and S_2 in interstellar ices. This paper is organized as follows. Section 2 presents spectroscopic information of the three targeted molecules. In particular, the data provided for H_2S_2 was not previously documented. Section 3 describes the observations that have been performed, while the results are shown in Sect. 4. The upper limits derived from our observations are discussed in Sect. 5. In Sect. 6 these upper limits are compared to the expected abundances from the experimental simulations with ice analogs, and in Sect. 7 to the estimated abundances from theoretical simulations taking into account the subsequent gas-phase chemistry. The conclusions are summarized in Sect. 8.

2. Laboratory spectroscopy of the sulfur-containing molecules in the gas phase

Disulfane, H_2S_2, also known as hydrogen disulfide, is a heavy homologue of hydrogen peroxide, H_2O_2. Whereas H_2O_2 displays large torsional splitting in the ground vibrational state, this splitting is hard to resolve for H_2S_2 even in the laboratory. It is an asymmetric top rotor very close to the prolate limit, i.e., its A rotational constant of almost 147 GHz is much larger than B and C, which are almost equal and slightly smaller than 6.97 GHz. Its dipole moment of about 1.1 D (Woon & Herbst 2009) is along the c-axis. The two equivalent H nuclei result in a 3:1 spin-statistical ratio between *ortho* and *para* levels which are described by K_c being odd and even, respectively. A large body of transition frequencies up to 421 GHz were taken from Behrend et al. (1990) with additional terahertz data from Belov et al. (1994) and Yamada et al. (1996). The precision of the data appeared to be 20 or 30 kHz for the most part. The $K = 3–2$ data in Belov et al. (1994) is too low compared with the data reported in Behrend et al. (1990) by about 300 kHz with rather small scatter. The absence of a reference signal in, e.g., Belov et al. (1994) could be an explanation, see SO data in Klaus et al. (1994) and Klaus et al. (1996). Therefore, the $K = 3–2$ data from Belov et al. (1994) were omitted from the fit. As a consequence, predicted transition frequencies should be viewed with some caution. As the result of this work, a catalog entry was created for the Cologne Database for Molecular Spectroscopy, CDMS, (Müller et al. 2001, 2005) with the spectroscopic information of this species, including predicted frequencies and intensities for its rotational transitions.

Elimination of one H atom from disulfane leads to the 2A″ thiosulfeno radical, $HS_2^{\cdot}$. The A rotational constant is roughly twice that of H_2S_2, while B and C are about 1 GHz larger. The dipole moment components were calculated as $\mu_a = 1.16$ D and $\mu_b = 0.83$ D (Peterson et al. 2008). Predictions of the $HS_2^{\cdot}$ rotational spectrum were also taken from the CDMS. They were based on the analysis of Tanimoto et al. (2000) which included lower frequency data from Yamamoto & Saito (1994). ^{1}H hyperfine structure is usually small and was often not resolved in the laboratory. Electron spin-rotation splitting is small for a-type transitions, e.g., on the order of 200 MHz and 1 GHz for $K_a = 0–0$ and $1–1$, respectively. It is several tens of gigahertz for b-type transitions.

Elimination of the second H atom yields S_2, the smallest molecule containing only sulfur. It is a heavy homologue of O_2, the ground electronic state is $^3\Sigma_g^-$. Because of its symmetry, it does not have an electric dipole moment, but it has a magnetic dipole moment which gives rise to a weak rotational spectrum. The selection rules are $\Delta N = 0, \pm 2$ and $\Delta J = 0, \pm 1$. The predictions were taken from the JPL catalog (Pickett et al. 1998). They are based on rotational data from Pickett & Boyd (1979) with additional ground state combination differences taken from the $b - X$ electronic spectrum (Fink et al. 1986). The magnetic g-factors were redetermined by Pickett & Boyd (1979). The rotational spectrum of O_2 is quite close to Hund's case (b), in which the three $\Delta N = 2$ transitions occur quite close in frequency.

Table 1. Targeted transitions and observational results.

Molecule	Transition	Frequency (MHz)	E_{up} (K)	g_{up}	A_{ul} (s^{-1})	Beam size ($''$)	rms[1] (K)	N (cm^{-2})
H_2S_2	$6_{1,5}$–$5_{0,5}$	**223 535.85**	20.8	39	4.23×10^{-5}	28	...	...[2]
H_2S_2	$13_{2,11}$–$14_{1,13}$	224 367.15	87.8	81	1.64×10^{-5}	28	0.0018	$\leq 1.7 \times 10^{15}$
H_2S_2	$13_{2,12}$–$14_{1,14}$	224 657.47	87.8	27	1.65×10^{-5}	28	...	...[2]
H_2S_2	$8_{1,7}$–$7_{0,7}$	**251 423.70**	30.8	51	5.92×10^{-5}	25	0.0026	$\leq 6.1 \times 10^{14}$
H_2S_2	$11_{2,9}$–$12_{1,11}$	252 271.50	71.0	69	2.25×10^{-5}	25	0.0025	$\leq 1.7 \times 10^{15}$
H_2S_2	$11_{2,10}$–$12_{1,12}$	252 486.63	71.0	23	2.25×10^{-5}	25	...	...[2]
H_2S_2	$10_{1,9}$–$9_{0,9}$	**279 312.25**	43.5	63	8.04×10^{-5}	22	...	...[2]
H_2S_2	$9_{2,7}$–$10_{1,9}$	280 174.30	57.0	57	2.94×10^{-5}	22	...	...[2]
H_2S_2	$9_{2,8}$–$10_{1,10}$	280 325.68	57.0	19	2.94×10^{-5}	22	0.0022	$\leq 3.7 \times 10^{15}$
H_2S_2	$14_{1,13}$–$13_{0,13}$	**335 087.32**	77.0	87	1.37×10^{-4}	19	...	...[2]
H_2S_2	$5_{2,3}$–$6_{1,5}$	335 971.39	36.9	33	4.05×10^{-5}	19	0.0036	$\leq 2.1 \times 10^{15}$
H_2S_2	$5_{2,4}$–$6_{1,6}$	336 029.02	36.9	11	4.05×10^{-5}	19	...	...[2]
HS_2^-	$16_{0,16,16,15}$–$15_{0,15,15,14}$[3]	252 270.66	103.1	31	1.22×10^{-4}	25	0.0028	$\leq 8.0 \times 10^{14}$
HS_2^-	$16_{0,16,16,16}$–$15_{0,15,15,15}$[3]	252 270.71	103.1	33	1.22×10^{-4}			
HS_2^-	$4_{1,3,5,4}$–$4_{0,4,5,4}$[3]	280 022.63	21.0	9	7.45×10^{-5}	22	0.0027	$\leq 1.6 \times 10^{15}$
HS_2^-	$4_{1,3,5,5}$–$4_{0,4,5,5}$[3]	280 023.28	21.0	11	7.49×10^{-5}			
HS_2^-	$21_{1,20,22,22}$–$20_{1,19,21,21}$[3]	333 247.58	189.7	45	2.84×10^{-4}	19	0.0052	$\leq 1.3 \times 10^{15}$
HS_2^-	$21_{1,20,22,21}$–$20_{1,19,21,20}$[3]	333 247.67	189.7	43	2.84×10^{-4}			
S_2	11_{10}–9_9	224 301.13	82.1	21	3.02×10^{-7}	28	0.0017	$\leq 2.2 \times 10^{16}$
S_2	15_{14}–13_{13}	333 685.77	126.3	29	7.78×10^{-7}	19	0.0039	$\leq 2.3 \times 10^{16}$

Notes. [(1)] rms is given in 5 km s^{-1} bins; [(2)] since these spectral regions present line contributions from other species near the frequency of the H_2S_2 transition, we have not used the corresponding noise rms value to compute the 1σ upper limits to the column density; [(3)] the last two quantum numbers designate the spin quanta.

The rotational splitting in S_2 is considerably smaller than in O_2 whereas the splitting caused mainly by the spin-spin coupling is much larger. As a consequence, the rotational spectrum is much more complex in its structure, closer to Hund's case (a) at low rotational quantum numbers N and closer to Hund's case (b) at higher N. Relatively strong transitions are those with $\Delta J = 0$, those with $\Delta N = 0$ are also comparatively strong.

3. Observations

The observations were carried out with the APEX 12 m telescope located at the high altitude site of Llano Chajnantor (Chile) in 2013, between August 30 and September 10, under good (PWV = 1.1−2.2 mm) weather conditions. We used the Swedish Heterodyne Facility Instruments (SHeFI; Vassilev et al. 2008) APEX-1 and APEX-2 as frontends with four different frequency setups of 4 GHz bandwidth each, covering a total of ∼16 GHz in a range of about 100 GHz. The eXtended bandwith Fast Fourier Transform Spectrometer (XFFTS; Klein et al. 2012) was used as backend. The XFFTS yields a spectral resolution of 76 KHz, which corresponds to ∼0.07−0.10 km s^{-1} in the spectral range observed.

The position-switching mode was chosen to perform the on/off observations. The on position was centered toward IRAS 16293-2422 A, $\alpha_{J2000} = 16^h32^{min}22.9^s$, $\delta_{J2000} = -24°28'37.0''$, while the off position was located at $\alpha_{J2000} = 16^h32^{min}09.4^s$, $\delta_{J2000} = -24°28'33.0''$, which is free of any $C^{18}O$ and ^{13}CO emission (Wakelam et al. 2004b). The half-power beamwidth of the telescope is ∼30−25$''$ for the APEX-1 receiver, and ∼23−17$''$ for the APEX-2 receiver. Therefore, emission from sources A and B of the binary protostellar system IRAS 16293-2422 could not be spatially resolved. The receivers were tuned to single sideband, and the intensities were measured in units of T_A^*. The conversion to T_{mb} was done by using main beam efficiencies of 0.75 and 0.73 for APEX-1 and APEX-2, respectively. Calibration and reduction of the data was previously performed with the software CLASS of the GILDAS package.

Our observations covered a total of 17 H_2S_2 transitions, 96 HS_2^- transitions, and 6 S_2 transitions. For H_2S_2, we selected the transitions with low upper level energy (a total of three transitions per frequency setup). The central frequency of the four observational setups corresponds to the frequencies of the selected H_2S_2 transitions expected to be the most intense in each setup, and are boldfaced in Table 1. For HS_2^- and S_2, we selected only those transitions with low upper level energy that fell in a clean region of the spectrum. The selected lines for H_2S_2, HS_2^-, and S_2 are listed in Table 1.

4. Results

Our observations toward the IRAS 16293-2422 hot corino reached root mean square (rms) values which are a factor 2−7 better than those reached by the TIMASS survey (Caux et al. 2011) in the 197 GHz−280 GHz frequency range, while they are comparable in the 328 GHz−366 GHz range. For the analysis of the spectra, we resampled the observations to a resolution of 0.5 km s^{-1}, and assumed a central radial velocity of v_{lsr} = 3.2 km s^{-1} for IRAS 16293 A (Jørgensen et al. 2011).

Lines detected at frequencies near those of the targeted transitions in Table 1 were assigned to previously detected species. The observed lines were then fitted with Gaussians (when possible, more than one Gaussian was used in the case of blended lines). For every putative assigned line, we used the integrated intensity extracted from the fit, and a simple model assuming local thermodinamical equilibrium to readily extract column densities that were compared with the column densities derived in previous works for the same species. This way, we could confirm the quality of our observations, and even assign lines

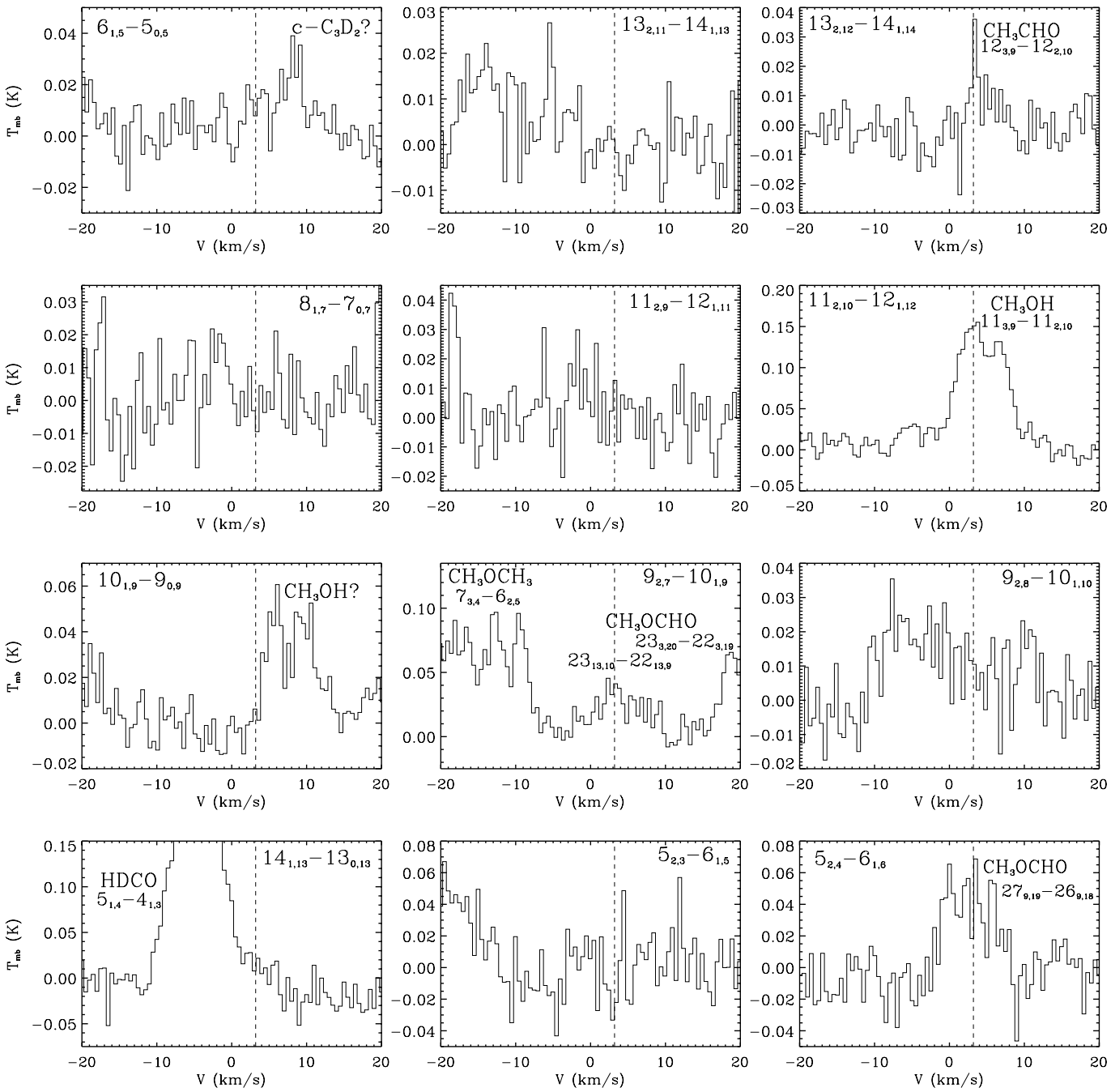

Fig. 1. Spectral windows where the H_2S_2 transitions listed in Table 1 should be detected. Vertical dashed lines mark a central radial velocity of v_{lsr} = 3.2 km s^{-1}, assumed for IRAS 16293 A (Jørgensen et al. 2011).

corresponding to previously detected species that were not documented in previous works (see Sect. 4.1).

Putative assignments of transitions corresponding to the targeted species were, however, ruled out because of missing lines (see Sect. 4.2).

4.1. Detection of species not containing sulfur

As mentioned above, we detected transitions from a collection of molecular species previously observed in other works such as $C^{17}O$, SO_2, HDCO, CH_3OH, CH_3CHO, CH_3OCHO, CH_3OCH_3, and others. Estimated column densities extracted from these emission lines are consistent with the column densities previously reported for these species (see, e.g., Cazaux et al. 2003; Caux et al. 2011). Some of these transitions are present in the spectral windows of Figs. 1 and 2 near the frequencies where the targeted transitions should be detected, and shortly described below.

Figure 1 shows one transition corresponding to CH_3CHO ($13_{2,12}$–$14_{1,14}$ panel) with E_{up} = 92.6 K, and one transition corresponding to HDCO ($14_{1,13}$–$13_{0,13}$ panel) with E_{up} = 56.3 K. The linewidth of the latter may indicate that HDCO is probing outflow material (IRAS 16293-2422 is embedded in the molecular cloud L1689N, which harbors multiple outflows; Wakelam et al. 2004b).

In the case of CH_3OH, one transition with E_{up} = 203 K is detected in the $11_{2,10}$–$12_{1,12}$ panel of Fig. 1. The double-peaked structure of the line may indicate that the emission is also originated in outflowing gas. The double-peaked line detected in

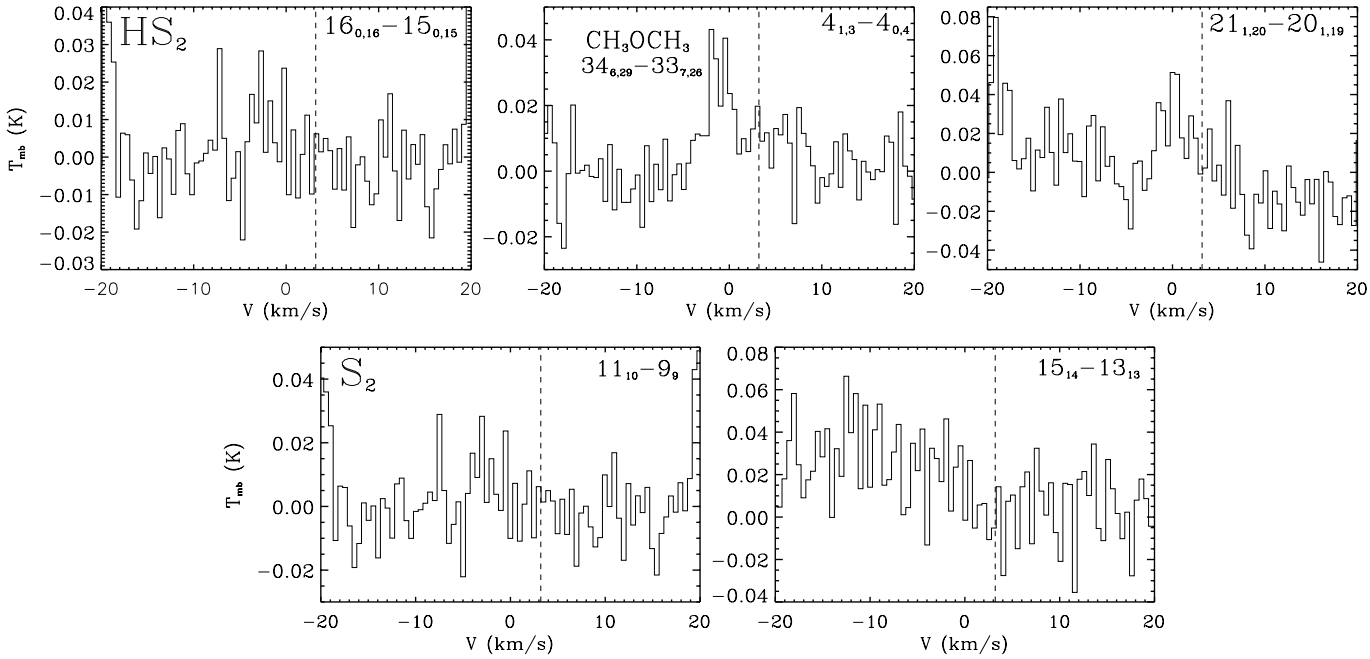

Fig. 2. Spectral windows where the HS_2^- (*top panels*) and S_2 (*bottom panels*) transitions listed in Table 1 should be detected. Vertical dashed lines mark a central radial velocity of v_{lsr} = 3.2 km s^{-1}, assumed for IRAS 16293 A (Jørgensen et al. 2011).

the $10_{1,9}$–$9_{0,9}$ panel of Fig. 1 may correspond to the 27_3–27_2 CH_3OH transition. However, the energy of this transition may be too high, even for an outflow (E_{up} = 926.1 K).

Four blended CH_3OCH_3 transitions with E_{up} = 38.2 K lead to three emission peaks in the $9_{2,7}$–$10_{1,9}$ panel of Fig. 1. They are possibly also blended with the $14_{11,4}$–$13_{11,3}$ H_2CCO transition (E_{up} = 113.9 K) that should appear at a slightly higher frequency and therefore at more blue-shifted velocities. The weaker $30_{4,26}$–$30_{3,27}$ CH_3OCH_3 transition is probably blended with the $23_{13,10}$–$22_{13,9}$ CH_3OCHO transition in that spectral window (E_{up} = 433.7 K and 462.6 K, respectively). Other four blended transitions with high upper level energy (E_{up} = 593.9 K) corresponding to dimethyl ether are detected in the $4_{1,3}$–$_{0,4}$ panel of Fig. 2.

Three more CH_3OCHO transitions are shown in Fig. 1, one in the $9_{2,7}$–$10_{1,9}$ panel (E_{up} = 173.2 K), and two blended transitions in the $5_{2,4}$–$6_{1,6}$ panel (E_{up} = 277.8 K for both transitions).

4.2. Non-detection of H_2S_2, HS_2^- or S_2

In Figs. 1 and 2, we show the spectral windows where the transitions listed in Table 1 should have been detected. The $6_{1,5}$–$5_{0,5}$ panel of Fig. 1 presents some emission centered at v_{lsr} ∼ 3.2 km s^{-1}, which may correspond to the $6_{1,5}$–$5_{0,5}$ transition of H_2S_2. However, the lack of detection of other transitions of this molecule prevents us from claiming this identification. In addition, the observed feature may present some contribution from the $18_{5,14}$–$17_{5,13}$ CH_3OCHO transition (E_{up} = 305.1 K). Other possible lines of HCOCN and NCHCCO could be overlapping with this emission. However, their frequencies are typically shifted by ∼0.5 MHz with respect to that of the H_2S_2 transition, which would imply an offset of ∼0.6 km s^{-1} in the v_{lsr}. The $14_{11,4}$–$14_{10,5}$ transition of c-C_3D_2 (an isotopologue not reported in Cazaux et al. 2003; and Caux et al. 2011) with E_{up} = 271.0 K could also contribute to the observed emission, since the uncertainty of the expected frequency is larger than 5 MHz.

For HS_2^- and S_2 (see Fig. 2), there are no clear emission features arising at the v_{lsr} of the source, except for the $4_{1,3}$–$4_{0,4}$ panel. However, as mentioned in Sect. 4.1, the detected feature is likely associated with four blended transitions of dimethyl ether.

From all this, we conclude that none of the transitions of H_2S_2, HS_2^- or S_2 observed toward IRAS 16293-2422 are detected. In Table 1, we provide the noise rms values over a linewidth of 5 km s^{-1} in the spectral region around the frequency of each transition. The measured rms values range from ∼1.8 to 5.2 mK, which provide stringent constraints on the upper limits to the molecular column densities and abundances of these species toward this low-mass warm core (see Sect. 5).

5. Upper limits to the column densities and abundances of H_2S_2, HS_2^- and S_2

From the 1σ rms values shown in Table 1, we have estimated the 1σ upper limits to the column densities and abundances of H_2S_2, HS_2^- and S_2 measured toward IRAS 16293-2422. To this purpose, we have used the simple model mentioned in Sect. 4, assuming that the emission of these molecules is optically thin, that their line profiles have linewidths of 5 km s^{-1}, and that the excitation temperature of the gas is 100 K. The column densities of the three species were subsequently corrected from beam dilution using the beam filling factor (Maret et al. 2011)

$$\eta = \frac{\theta_{source}^2 + \theta_{beam}^2}{\theta_{source}^2} \quad (1)$$

and considering a source extension of 2″ in diameter (Wakelam et al. 2004b). In addition, the 1σ upper limits for HS_2^- are computed taken into account that the three pairs of lines cannot be resolved in our observations.

The upper limits to the column densities of H_2S_2, HS_2^- and S_2 are shown in the last column of Table 1. The most stringent values are ≤6.1 × 10^{14} cm^{-2}, ≤8.0 × 10^{14} cm^{-2}, and ≤2.2 × 10^{16} cm^{-2} respectively (see also Table 2, Col. 2).

Table 2. Upper limits to the column densities and molecular abundances of H_2S_2, $HS_2^{\cdot}$, and S_2 estimated from the observations, and abundances calculated in laboratory experiments.

Molecule	N_{mol} (cm^{-2})	$N_{mol}/N(H_2)$	$[N_{mol}/N(H_2S)]_{obs}$ (%)	$[N_{mol}/N(H_2S)_i]_{lab}$ [1] (%)
H_2S_2	$\leq 6.1 \times 10^{14}$	$\leq 8.1 \times 10^{-9}$	≤ 1.5	≤ 25.0 [2]
$HS_2^{\cdot}$	$\leq 8.0 \times 10^{14}$	$\leq 1.1 \times 10^{-8}$	≤ 2.0	15.0
S_2	$\leq 2.2 \times 10^{16}$	$\leq 2.9 \times 10^{-7}$	≤ 55.0	...[3]

Notes. [(1)] After irradiation of pure H_2S ices with a total fluence of $\sim 1.5 \times 10^{18}$ photons cm^{-2}. Abundances are relative to the initial H_2S in the experiments. Derived from Jiménez-Escobar et al. (2012). [(2)] This upper limit is estimated considering that all the sulfur atoms not contained in H_2S or $HS_2^{\cdot}$ molecules at the end of the experiments reported in Jiménez-Escobar et al. (2012) are forming H_2S_2. [(3)] S_2 was not quantified since it was detected by mass spectrometry during warm-up of the UV-processed ice analogs in Jiménez-Escobar et al. (2012), but not by infrared spectroscopy.

The upper limits to the abundance of these molecules with respect to H_2 are derived by using an H_2 column density of $N(H_2) = 7.5 \times 10^{22}$ cm^{-2} (Ceccarelli et al. 2000) These upper limits are shown in Col. 3 of Table 2 and are $\leq 8.1 \times 10^{-9}$ for H_2S_2, $\leq 1.1 \times 10^{-8}$ for $HS_2^{\cdot}$, and $\leq 2.9 \times 10^{-7}$ for S_2.

Since no molecule with a sulfur-sulfur bond has been detected so far in the interstellar medium, the estimated upper limits can be compared only to the abundances of species with just one sulfur atom. In this case, we have calculated the upper limits to the abundance of these species with respect to H_2S in the same source, which is thought to be the parent molecule of the targeted species. We have considered an H_2S column density of $N(H_2S) = 4 \times 10^{16}$ cm^{-2} as reported in Wakelam et al. (2004b). The relative upper limits are shown in Col. 4 of Table 2 and are $\leq 1.5\%$, $\leq 2.0\%$ and $\leq 55.0\%$ for H_2S_2, $HS_2^{\cdot}$ and S_2, respectively, which leads to a rough upper limit of about 1% of S-S bonded species with respect to those with only one S atom.

6. Comparison with laboratory H_2S-bearing ice irradiation experiments

The upper limits to the abundances relative to H_2S are compared to the values expected from the laboratory experiments performed by Jiménez-Escobar & Muñoz Caro (2011), also shown in Table 2 (Col. 5). The measured upper limits are factors of 7−17 lower than the abundances measured in the experiments.

Differences between experimental and observed abundances could arise, on one hand, from the differences between the experimental simulations performed in the laboratory and the real processes taking place in the interstellar and circumstellar medium, leading to an overestimation of the expected abundances, as it is explained below. The laboratory simulations reported in Jiménez-Escobar & Muñoz Caro (2011) used to derive the abundances shown in the fifth column of Table 2 were carried out with pure H_2S ices. However, solid H_2S is expected to be found in a water-rich environment in the interstellar and circumstellar medium, along with other hydrogenated species (Allamandola et al. 1999; Jiménez-Escobar & Muñoz Caro 2011). Since H_2S has not been firmly detected in interstellar or circumstellar ices, this scenario remains to be confirmed, but processing of solid H_2S could take place to a limited extent in multicomponent ices. In the dense interstellar medium, solid H_2S can be processed in dense cloud interiors by the secondary UV-field produced by excitation of H_2 molecules by cosmic rays, and/or by the radiation emitted by the central object in hot cores and hot corinos. During the experiments in Jiménez-Escobar et al. (2012), pure H_2S ice analogs experienced a total fluence of $\sim 1.5 \times 10^{18}$ UV-photons cm^{-2}, which is higher than the fluence of $\sim 3.2 \times 10^{17}$ photons cm^{-2} that ice mantles are expected to experience in dense cloud interiors after 10^6 yr, assuming a flux value of 10^4 photons cm^{-2} s^{-1} for the secondary UV-field (Shen et al. 2004, and ref. therein).

On the other hand, the region affected by the X-ray radiation emitted by a protostar like IRAS 16293 A, with a typical extension of ∼10 AU (Ciaravella et al. 2011), is smaller than the region where the sulfur-containing species are expected to be detected in these observations (with an extension of ∼230 AU for an assumed source size of 2″ in diameter; Wakelam et al. 2004b). Therefore, the upper limits shown in the third and fourth columns of Table 2 could be affected by beam dilution, (and, therefore, be underestimated) if the sulfur-bearing molecules were confined to the region affected by the X-ray emitted by the protostars in IRAS 16293-2422.

Finally, H_2S_2 and $HS_2^{\cdot}$, although efficiently produced in ices, may undergo an active gas-phase chemistry once desorbed from dust grains. This could lower the gas-phase abundances of these species to undetectable levels. This possibility is further explored in Sect. 7.

7. Chemical modeling of H_2S_2, $HS_2^{\cdot}$ and S_2 in IRAS 16293-2422

In a recent paper, Woods et al. (2015) have incorporated the experimental data of Garozzo et al. (2010) on the production of the S-bearing species H_2S_2, $HS_2^{\cdot}$ and S_2 in ices, into the UCL_CHEM chemical code (Viti & Williams 1999; Viti et al. 2004). In these experiments, Garozzo et al. (2010) bombarded a CO:H_2S = 10:1 mixture sample with 200 keV protons simulating the impact of cosmic rays on interstellar ice analogs. Although the irradiation source is different from the ones used in Jiménez-Escobar & Muñoz Caro (2011) and Jiménez-Escobar et al. (2014), we note that the measured production of H_2S_2 in the ices at low fluences is about 30%, i.e., similar within 5% to the one obtained in the experiments with UV-photon and X-ray irradiation (see Table 2). Since we are interested in the chemistry of these sulfur-bearing species in the gas phase after thermal desorption, a small difference in the H_2S_2 production by 5% is not expected to have a noticeable effect in the final results. We therefore made use of this new chemical network to test whether gas-phase chemistry is responsible for the lack of detection of H_2S_2, $HS_2^{\cdot}$ and S_2 toward IRAS 16293.

The UCL_CHEM gas-grain chemical code is a two-phase model. In Phase I, this code simulates the free-fall gravitational collapse of a cloud where the mantles of dust grains form self-consistently via freeze-out reactions. In our modeling, we have considered two groups of freeze-out reactions for the sulfur

Table 3. Models run for the chemistry of H_2S_2, HS_2^- and S_2 toward IRAS 16293.

Model	n_{H_2} (cm^{-3})	f_s	Freeze-out reactions group	Reactions[1]
(a)	1×10^7	1.3×10^{-5}	1	50% $HS_2 \rightarrow mHS_2$ 50% $HS_2 \rightarrow mH_2S_2$ 50% $H_2S_2 \rightarrow mH_2S_2$ 50% $H_2S_2 \rightarrow mHS_2$
(b)	1×10^8	1.3×10^{-5}	1	50% $S \rightarrow mHS$ 50% $S \rightarrow mH_2S$ 0% $S \rightarrow mS$
(c)	1×10^7	1.4×10^{-6}	1	50% $HS_2 \rightarrow mHS_2$ 50% $HS_2 \rightarrow mH_2S_2$ 50% $H_2S_2 \rightarrow mH_2S_2$ 50% $H_2S_2 \rightarrow mHS_2$
(d)	1×10^8	1.4×10^{-6}	1	50% $S \rightarrow mHS$ 50% $S \rightarrow mH_2S$ 0% $S \rightarrow mS$
(e)	1×10^7	1.3×10^{-5}	2	100% $HS_2 \rightarrow mHS_2$ 0% $HS_2 \rightarrow mH_2S_2$ 100% $H_2S_2 \rightarrow mH_2S_2$ 0% $H_2S_2 \rightarrow mHS_2$
(f)	1×10^8	1.3×10^{-5}	2	0% $S \rightarrow mHS$ 0% $S \rightarrow mH_2S$ 100% $S \rightarrow mS$

Notes. [(1)] mH_2S_2, mHS_2, mH_2S, and mS refers to species frozen onto the mantles of dust grains.

species: one group where molecules can either freeze onto grains as themselves, or undergo hydrogenation/dehydrogenation reactions in the ices; and a second group where species freeze onto grains only as themselves (see Table 3 for the freeze-out reactions considered in the models). The formation of the initial core occurs from a diffuse medium with H_2 densities of $\sim$100 cm^{-3} and the collapse stops when the final density is reached in the model. The UCL_CHEM is run for two final densities of 10^7 cm^{-3} and 10^8 cm^{-3}, covering the range of H_2 gas densities typically assumed for low-mass warm cores (see, e.g., Awad et al. 2010). Finally, in order to test the effects of the presence of a sulfur residue in dust grains in the form of S_8 or of any other type of aggregate (see Jiménez-Escobar & Muñoz Caro 2011), we also considered two models with different initial sulfur abundances (see Table 3): one assuming the solar sulfur abundance ($f_s = 1.318 \times 10^{-5}$; Asplund et al. 2009) and a second model considering a depleted abundance of sulfur ($f_s = 1.4 \times 10^{-6}$; Sofia et al. 1994). In Phase II, UCL_CHEM calculates the time-dependent evolution of the chemistry of gas and dust once stellar activity is present. As explained in Viti et al. (2004), molecular species are thermally evaporated after the turning on of the protostar in different temperature bands. Here, we follow the classification proposed by Woods et al. (2015) where H_2S, HS and H_2S_2 are considered as *intermediate* species evaporating at temperatures between 80 K–90 K, and where HS_2^- is a *reactive* molecule that co-desorbs with water at around 100 K. The maximum temperature assumed for IRAS 16293 in Phase II is 100 K (Ceccarelli et al. 2000). In our models the temperature increases monotonically following the prescription of Viti et al. (2004). We also assume a standard cosmic ray ionisation rate ($\zeta = 1.3 \times 10^{-17}$ s^{-1}) for all models.

In Fig. 3, we report the abundances of all major species involved in the sulfur chemistry toward IRAS 16293. Consistently with the results of Woods et al. (2015), the level of hydrogenation of the ice species in Phase I does not significantly affect the abundances of these species in Phase II. Gas phase reactions after ice desorption clearly dominate the chemistry of S-bearing species. The abundances of H_2S_2, HS_2^- and S_2 in the mantles at the end of Phase I indeed differ by only factors of a few between the two freeze-out cases considered in our models. Therefore, in Fig. 3 we only show the modeling results for the cases where molecules freeze out both as themselves or undergoing hydrogenation/dehydrogenation in the ices (see Group 1 reactions in Table 3). Differences are found between models with different H_2 gas densities (see, e.g., models a and b). In particular, the abundances of H_2S_2, HS_2^- and S_2 are factors 1.7–6.7 higher in the models with $n_{H_2} = 10^7$ cm^{-3} than for H_2 gas densities of 10^8 cm^{-3}. One explanation is that more H_2S is formed on grain surfaces at higher densities, which in turn is converted into SO_2 via the surface reaction $H_2S + 2O \rightarrow SO_2 + H_2$ (see Table 3 in Woods et al. 2015). Since H_2S preferentially goes into SO_2 at high densities, there is a smaller amount of this molecule available in the ices for the production of H_2S_2, HS_2^- and S_2, leading to lower abundances of the latter species. As expected, Fig. 3 also shows that a depleted initial abundance of atomic sulfur yields lower abundances in Phase II for all S-bearing species considered in our modeling.

In order to compare the model results with our upper limits of Sect. 5, we need to inspect the abundances of H_2S_2, HS_2^- and S_2 at time-scales $\sim 10^5$ yrs inferred for the IRAS 16293 low-mass warm core (see André et al. 1993). The predicted abundances of these species for models (a), (b), (c), and (d) are shown in Table 4 along with the upper limits derived from our observations. For the models with a sulfur solar abundance (models (a) and (b)), higher H_2 densities of 10^8 cm^{-3} fit better the observations (see Table 4). However, for models (c) and (d) where the initial sulfur abundance is depleted, we find that the predicted abundances of H_2S_2, HS_2^- and S_2 lie within the upper limits measured toward IRAS 16293. Therefore, even in the absence of a sulfur residue, our modeling shows that gas-phase chemistry can explain the lack of detection of H_2S_2, HS_2^- and S_2 toward this source.

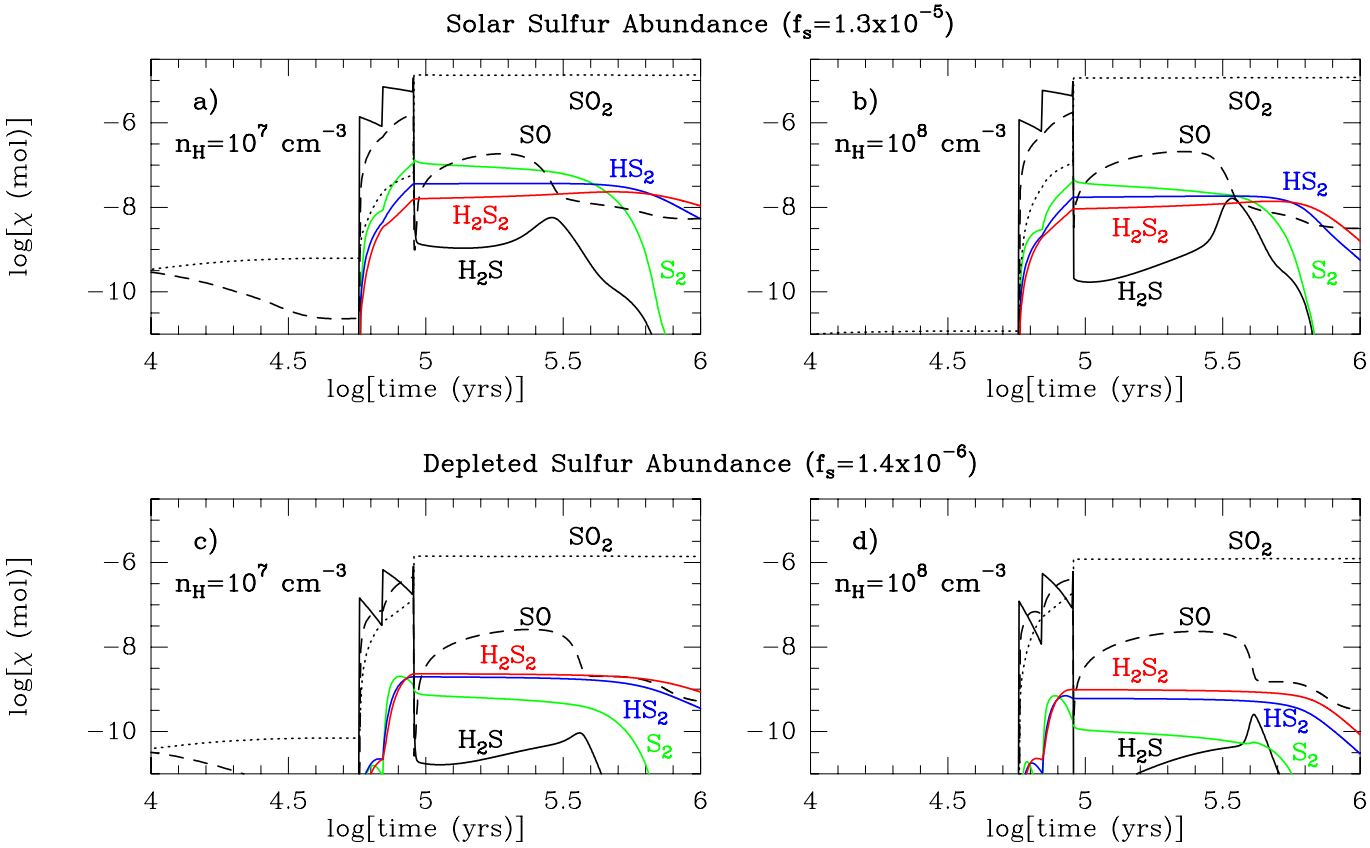

Fig. 3. Time-dependent evolution of abundances of selected sulfur-bearing species in IRAS 16293 according to the UCL_CHEM code for models **a)**, **b)**, **c)**, and **d)**, whose most important parameters are shown in Table 3. Colored lines correspond to the targeted species. Black solid line is for H_2S. Black dashed and dotted lines correspond to SO and SO_2, respectively.

Table 4. Comparison of the modelled H_2S_2, HS_2 and S_2 abundances with the upper limits derived from the observations.

Molecule	N_{mol} (cm^{-2}) Model (a)	N_{mol} (cm^{-2}) Model (b)	N_{mol} (cm^{-2}) Model (c)	N_{mol} (cm^{-2}) Model (d)	Observations
H_2S_2	1.6×10^{-8}	9.3×10^{-9}	2.3×10^{-9}	1.0×10^{-9}	$\leq 8.1 \times 10^{-9}$
HS_2	3.6×10^{-8}	1.7×10^{-8}	2.0×10^{-9}	6.2×10^{-10}	$\leq 1.1 \times 10^{-8}$
S_2	1.1×10^{-7}	3.7×10^{-8}	7.4×10^{-10}	1.1×10^{-10}	$\leq 2.9 \times 10^{-7}$

8. Conclusions

A fraction of the missing sulfur in the interstellar medium is thought to be locked in the ice mantles on dust grains. Interstellar ice mantles are energetically processed, leading to chemical and structural changes. Previous laboratory experiments simulating the irradiation of H_2S-containing ice analogs under astrophysically relevant conditions lead to the production of H_2S_2, HS_2, and S_2 among other species. These molecules would be subsequently released to the gas phase by non-thermal desorption in dense clouds, and also by thermal desorption in regions around YSOs. We have presented the first single-dish observations targeting a wide selection of rotational transitions predicted for the S-S bonded molecules H_2S_2, HS_2, and S_2 toward the low-mass warm core IRAS 16293-2422, a region with an active chemistry and a high H_2S gas-phase abundance. As a result of this work, the predicted rotational spectrum of H_2S_2 was made available as a new entry in the CDMS catalog. Although none of the species were firmly detected, we have estimated an upper limit to their molecular abundances of $\leq 8.1 \times 10^{-9}$, $\leq 1.1 \times 10^{-8}$, and $\leq 2.9 \times 10^{-7}$ relative to H_2 or $\leq 1.5 \times 10^{-2}$, $\leq 2.0 \times 10^{-2}$, and $\leq 5.5 \times 10^{-1}$ relative to H_2S, respectively. These abundances are therefore up to two orders of magnitude lower than the observed abundance of H_2S in the same source, which is thought to be the parent molecule of species with a disulfide (S-S) bond. The estimated upper limits are one order of magnitude lower than the abundances found in the experimental simulations. This could be the result of an underestimation of the measured upper limits caused by beam dilution of their emitting regions, or an overestimation of the expected abundances from the laboratory experiments. Although experimental simulations try to mimick interstellar conditions, differences between the ice analogs and the interstellar ice mantles, the densities in the UHV chamber and the interstellar and circumstellar regions, and the processing time of the samples are inevitable. On the other hand, subsequent gas-phase chemistry after desorption could have reduced the gas-phase abundances of these species to undetectable levels in our observations. Future high-angular resolution observations will establish whether these species are truly depleted in the gas phase or whether their emitting regions are largely diluted in our single-dish observations.

Acknowledgements. This research was financed by the Spanish MINECO under project AYA2011-29375. R.M.-D. benefited from a FPI grant from

Spanish MINECO. I.J.-S. acknowledges the funding received from the People Programme (Marie Curie Actions) of the European Union's Seventh Framework Programme (FP7/2007−2013) under REA grant agreement PIIF-GA-2011-301538, and from the STFC through an Ernest Rutherford Fellowship (proposal number ST/L004801/1).

References

Allamandola, L. J., Bernstein, M. P., Sandford, S. A., & Walker, R. L. 1999, Space Sci. Rev., 90, 219
André, P., Ward-Thompson, D., & Barsony, M. 1993, ApJ, 406, 122
Asplund, M., Grevesse, N., Sauval, A. J., & Scott, P. 2009, ARA&A, 47, 481
Awad, Z., Viti, S., Collings, M. P., & Williams, D. A. 2010, MNRAS, 407, 2511
Behrend, J., Mittler, P., Winnewisser, G., Yamada, K. M. T., & Winnewisser, M. 1990, J. Mol. Spectr., 141, 265
Belov, S. P., Liedtke, M., Klaus, T., et al. 1994, J. Mol. Spectr., 166, 489
Bockelée-Morvan, D., Lis, D. C., Wink, J. E., et al. 2000, A&A, 353, 1101
Boogert, A. C. A., Schutte, W. A., Helmich, F. P., Tielens, A. G. G. M., & Wooden, D. H. 1997, A&A, 317, 929
Caux, E., Kahane, C., Castets, A., et al. 2011, A&A, 532, A23
Cazaux, S., Tielens, A. G. G. M., Ceccarelli, C., et al. 2003, ApJ, 593, L51
Ceccarelli, C., Castets, A., Caux, E., et al. 2000, A&A, 355, 1129
Charnley, S. B. 1997, ApJ, 481, 396
Ciaravella, A., Jiménez-Escobar, A., Muñoz Caro, G. M., et al. 2011, ApJ, 746, L1
Doty, S. D., van Dishoeck, E. F., & Tan, J. 2004, BAAS, 36, 1505
Ferrante, R. F., Moore, M. H., Spiliotis, M. M., & Hudson, R. L. 2008, ApJ, 684, 1210
Fink, E. H., Kruse, H., & Ramsay, D. A. 1986, J. Mol. Spectr., 119, 377
Garozzo, M., Fulvio, D., Kanuchova, Z., Palumbo, M. E., & Strazzulla, G. 2010, A&A, 509, A67
Geballe, T. R., Baas, F., Greenberg, J. M., & Schutte, W. 1985, A&A, 146, L6
Grim, R. J. A., & Greenberg, J. M. 1987, A&A, 181, 155
Hatchell, J., Thompson, M. A., Millar, & MacDonald, G. H. 1998, A&A, 338, 713
Jansen, D. J., Spaans, M., Hogerheijde, M. R., & van Dishoeck, E. F. 1995, A&A, 303, 541
Jiménez-Escobar, A., & Muñoz Caro, G. M. 2011, A&A, 536, A91
Jiménez-Escobar, A., Muñoz Caro, G. M., Cicarelli, A., et al. 2012, ApJ, 751, L40
Jiménez-Escobar, A., Muñoz Caro, G. M., & Chen, Y.-J. 2014, MNRAS, 443, 343
Jiménez-Serra, I., Zhang, Q., Viti, S., Martín-Pintado, J., & de Wit, W.-J. 2012, ApJ, 753, 34
Jørgensen, J. K, Bourke, T. L., Nguyen Luong, Q., & Takakuwa, S. 2011, A&A, 534, A100
Klaus, T., Belov, S. P., Saleck, A. H., Winnewisser, G., & Herbst, E. 1994, J. Mol. Spectr., 168, 235
Klaus, T., Saleck, A. H., Belov, S. P., et al. 1996, J. Mol. Spectr., 180, 197
Klein, B., Hochgürtel, S., Krämer, I., et al. 2012, A&A, 542, L6
Maret, S., Hily-Blant, P., Pety, J., Bardeau, S., & Reynier, E. 2011, A&A, 526, A47
Millar, T. J., & Herbst E. 1990, A&A, 231, 466
Moore, M. H., Hudson, R. L., & Carlson, R. W. 2007, Icarus, 189, 409
Müller, H. S. P., Thorwirth, S., Roth, D. A., & Winnewisser, G. 2001, A&A, 370, L49
Müller, H. S. P., Schlöder, F., Stutzki, J., & Winnewisser, G. 2005, J. Mol. Struct., 742, 215
Mundy. L. G., Wootten, A., Wilking, B. A., Blake, G. A., & Sargent, A. I. 1992, ApJ, 385, 306
Muñoz Caro, G. M., Jiménez-Escobar, A., Martín-Gago, J. Á., et al. 2010, A&A, 522, A108
Palumbo, M. E., Tielens, A. G. G. M., & Tokunaga, A. T. 1995, ApJ, 449, 674
Peterson, K. A., Mitrushchenkov, A., & Francisco, J. S. 2008, Chem. Phys., 346, 34
Pickett, H. M., & Boyd, T. L. 1979, J. Mol. Spectr., 75, 53
Pickett, H. M., Poynter, R. L., Cohen, E. A., et al. 1998, J. Quant. Spectr. Rad. Transf., 60, 883
Ruffle, D. P., Hartquist, T. W., Caselli, P., & Williams, D. A. 1999, MNRAS, 306, 691
Smith, R. G. 1991, MNRAS, 249, 172
Tanimoto, M., Klaus, T., Müller, H. S. P., & Winnewisser, G. 2000, J. Mol. Spectr., 199, 73
Tieftrunk, A., Pineau des Forets, G., Schilke, P., & Walmsley, C. M. 1994, A&A, 289, 579
Shen, C. J., Greenberg, J. M., Schutte, W. A., & van Dishoeck, E. F. 2004, A&A, 415, 203
Sofia, U. J., Cardelli, J. A., & Savage, B. D. 1994, ApJ, 430, 650
van der Tak, F. F. S, Boonman, A. M. S., Braakman, R., & van Dishoeck, E. F. 2003, A&A, 412, 133
Vassilev, V., Meledin, D., Lapkin, I., et al. 2008, A&A, 490, 1157
Viti, S., & Williams, D. A. 1999, MNRAS, 305, 4, 755
Viti, S., Caselli, P., Hartquist, T. W., & Williams, D. A. 2001, A&A, 370, 1017
Viti, S., Collings, M. P., Dever, J. W., McCoustra, M. R. S., & Williams, D. A. 2004, MNRAS, 354, 1141
Wakelam, V., Caselli, P., Ceccarelli, C., Herbst, E., & Castets, A. 2004a, A&A, 422, 159
Wakelam, V., Castets, A., Ceccarelli, C., et al. 2004b, A&A, 413, 609
Wakelam, V., Hersant, F., & Herpin, F. 2011, A&A, 529, A112
Woods, P. M., Occhiogrosso, A., Viti, S., et al. 2015, MNRAS, 450, 1256
Woon, D. E., & Herbst, E. 2009, ApJSS, 185, 273
Yamada, K. M. T., Behrend, J., Belov, S. P., & Winnewisser, G. 1996, J. Mol. Spectr., 176, 397
Yamamoto, S., & Saito, S. 1994, Can. J. Phys., 72, 954